

Neutral Current $1\pi^0$ Production at MiniBooNE

C. E. Anderson, for the MiniBooNE collaboration

Yale University; New Haven, CT 06520

Abstract. We describe the analysis employed in measuring neutral current single π^0 production at MiniBooNE and report the first absolute differential cross sections (as functions of π^0 angle and π^0 momentum). We find total flux-averaged cross sections of $(4.73 \pm 0.05_{stat} \pm 0.40_{sys}) \times 10^{-40} \text{ cm}^2$ and $(1.42 \pm 0.05_{stat} \pm 0.14_{sys}) \times 10^{-40} \text{ cm}^2$ for ν_μ and $\bar{\nu}_\mu$ induced NC $1\pi^0$ production, respectively. We also include a measurement of the total cross section for ν_μ -induced exclusive resonant NC $1\pi^0$ production.

PACS: 13.15.+g, 25.30.Pt

INTRODUCTION

The MiniBooNE experiment is a ν_e -appearance oscillation search that couples the Booster Neutrino Beam (BNB) at Fermilab with a 12.2 m diameter, mineral oil-filled Cherenkov detector[1]. Operating in neutrino mode, the BNB produces a 93.6% pure ν_μ beam with mean energy 808 MeV. In antineutrino mode, a 83.73% pure $\bar{\nu}_\mu$ beam with mean energy 630 MeV and considerable wrong-sign (ν_μ) contamination is produced.[2] Two optically separated regions comprise the detector: a 5.75 m radius inner tank and a veto region extending 0.35 m beyond it. The tank is instrumented with 1280 inward-facing 8 inch photomultiplier tubes (PMTs) providing 11.3% photocathode coverage and the veto region is instrumented with 240 additional PMTs.

We define neutral current single π^0 (NC $1\pi^0$) events to be those neutral current interactions in which exactly one π^0 and no other mesons exits the struck nucleus. Since the π^0 decays nearly instantaneously to two photons, the expected signature in the detector is two Cherenkov rings from showering particles. The two exclusive NC $1\pi^0$ channels (resonant and coherent production) are the principal sources of NC $1\pi^0$ production. Resonant production ($\nu + N \rightarrow \nu + (\Delta, N^*), (\Delta, N^*) \rightarrow N' + \pi^0$) occurs via the excitation of a nucleon resonance (usually the $\Delta(1232)$ at $E_\nu < 2 \text{ GeV}$) that decays via emission of a π^0 and nucleon. In coherent production ($\nu + A \rightarrow \nu + A + \pi^0$), the neutrino scatters coherently off the nucleus as whole. Such scattering necessarily leaves the nucleus in the ground state, which requires that coherent production typically occur at lower Q^2 . Final state interactions (FSI) such as pion absorption and charge exchange can radically alter the makeup of the final state; events in the exclusive channels may not be classified as NC $1\pi^0$ events and events outside the exclusive channels may morph into NC $1\pi^0$ events (*e.g.* a π^\pm can become a π^0 via charge exchange).

The v3 NUANCE event generator[3] together with a GEANT3-based detector Monte Carlo are used for simulation at MiniBooNE. Models by Rein & Sehgal (R-S) are used to simulate the two exclusive NC $1\pi^0$ production channels—resonant[4] and coherent[5]. R-S resonant production includes the contribution from the dominant $\Delta(1232)$ resonance as well as 17 higher mass resonances and their interferences. Unlike in the R-S model, the NUANCE implementation of R-S resonant production decays all resonance isotropically. We further correct the angular distribution of decaying spin- $\frac{3}{2}$ resonances such that it is non-isotropic according to the R-S model[4]. The implementation of the R-S coherent model differs from the model in two ways. First, the absorptive factor accounting for pion interactions in the nucleus is replaced with the NUANCE FSI model. Second, the amount of coherent production is scaled by a factor of 0.65 per an earlier *in situ* measurement of this value[6]. We use axial masses of $M_A^{1\pi(res)} = 1.1 \text{ GeV}/c^2$ and $M_A^{1\pi(coh)} = 1.03 \text{ GeV}/c^2$ for the generation of resonant and coherent interactions, respectively. Monte Carlo predicts the composition of NC $1\pi^0$ signal events in terms of exclusive interaction channels in neutrino(antineutrino) mode to be as follows: 77%(59%) NC resonant $1\pi^0$ production, 17%(38%) NC coherent $1\pi^0$ production, 2%(2%) NC π^\pm production, 2%(< 1%) NC elastic scattering, and < 1%(< 1%) each multi-pion, deep inelastic scattering (DIS), and K, ρ , η production.

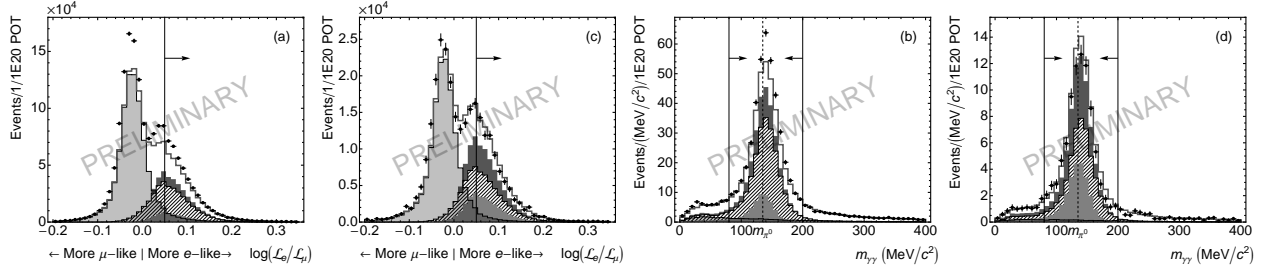


FIGURE 1. (a) Distribution of the difference between the e log-likelihood and the μ log-likelihood for events passing cuts (1)-(4) described in the text for neutrino running. Monte Carlo is depicted by a dark-gray line and data by black dots. Both data and Monte Carlo are absolutely normalized to 10^{20} POT. Error bars are statistical. Also shown are the contributions from π^0 -absent events (translucent light-gray fill), NC $1\pi^0$ production (dark-gray fill), resonant NC π^0 production (hatched fill), and coherent NC π^0 production (gray fill). Candidate NC $1\pi^0$ events are in the region indicated by the arrows. (b) The same for antineutrino running. (c) Distribution of the reconstructed $\gamma\text{-}\gamma$ invariant mass for events passing cuts (1)-(6) described in the text in neutrino running. (d) The same for antineutrino running.

CANDIDATE SELECTION

Reconstruction is preceded by a series of preliminary cuts. PMT hits are clustered according to time. Each cluster is identified as a subevent. Since muon decay electrons, *i.e.* a strong indicator of a charge current (CC) event, are the usual source of multiple subevents, the first cut requires that (1) events have only one subevent and that the subevent reside in the beam window. To eliminate uncontained events as well as events with cosmic muons entering the tank in the beam window, events are required to possess (2) less than 6 PMT hits in the veto region. Additionally events must have (3) more than 200 PMT hits in the tank region. This requirement reduces the background from NC elastic events and eliminates events with a decay Michel electron from a cosmic muon entering the tank before the beam window.

After preliminary cuts, the remaining events undergo reconstruction in order to measure kinematic variables and perform particle identification. The reconstruction algorithm takes the form of a track-based, least negative-log-likelihood (NLL) fit performed under multiple particle hypotheses[7]. For each event, the fit finds the kinematic configuration of hypothesized tracks that minimizes the NLL of the predicted of PMT hits (formed from predicted Cherenkov and scintillation light emission in the tank) *vis-à-vis* the data. Three hypotheses are used in this analysis: one-track electron (e) and muon (μ) hypotheses and a two-track pion (π^0) hypothesis in which the invariant mass of the tracks (treated as photons) can be fixed to the π^0 mass or left unconstrained. After reconstruction, a fiducial volume cut is made. Candidates must (4) reside within 500 cm of the center of the tank according to the electron fit. The next two cuts use the hypothesis likelihoods. (5) Candidates must be more electron-like than muon-like and (6) more pion-like than electron-like. More specifically $\log(\mathcal{L}_e/\mathcal{L}_\mu) > 0.05$ and $\log(\mathcal{L}_e/\mathcal{L}_\pi) < 0$. The distribution of the difference between the electron NLL and the muon NLL appears in Figure 1. The separation between events with and without a π^0 is quite clear. Last, we require that (7) the invariant mass extracted from unconstrained pion fit be near the π^0 mass (between 80 and 200 MeV/c^2). A well-defined peak around the π^0 mass of $134.97 \text{ MeV}/c^2$ is visible in Figure 1. With 6.461×10^{20} protons-on-target (POT) collected in neutrino running, 21375 events pass cuts. 2290 events pass cuts from antineutrino running with 3.386×10^{20} POT collected. Monte Carlo overestimates the number of events passing cuts in neutrino mode by a factor of $1.109(8)_{\text{stat}}$ and underestimates it in antineutrino mode by a factor of $0.94(2)_{\text{stat}}$.

ANALYSIS & RESULTS

Photon kinematics extracted by the π^0 fit are used to derive the π^0 kinematics. The π^0 momentum is simply the sum of the reconstructed momentum of the two photons. We assume the incoming neutrino is traveling in the beam direction, which is oriented with the z -axis by convention, so the π^0 angle is taken to be the angle relative to the z -axis. Histograms of π^0 momentum (p_{π^0}) and the cosine of the π^0 angle ($\cos\theta_{\pi^0}$) are filled with the NC $1\pi^0$ candidates. These histograms appear in Figure 2. The neutrino mode π^0 momentum distribution extends to $1.5 \text{ GeV}/c$ while the antineutrino mode distribution extends to $1.1 \text{ GeV}/c$.

The selection cuts result in a sample possessing a signal fraction of 73% in neutrino mode and 57% in antineutrino

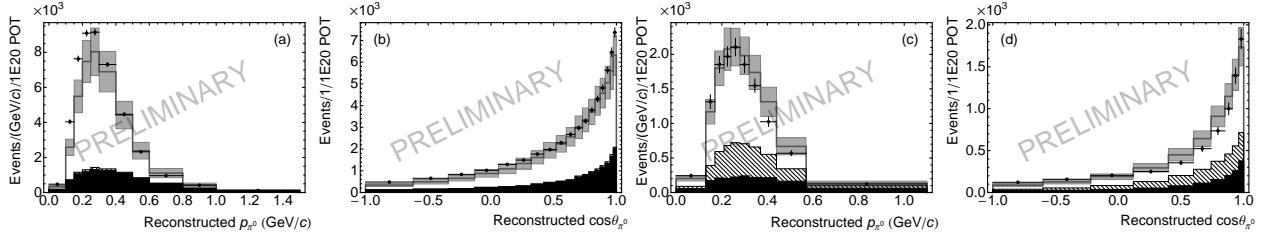


FIGURE 2. (a) The reconstructed π^0 momentum distribution for NC $1\pi^0$ candidates in neutrino running. The Monte Carlo distribution is shown as a dark-gray line and data as black dots. The box histogram is the systematic error on the Monte Carlo distribution; the error bars on the data are statistical. Distributions are absolutely normalized to 10^{20} POT. The black filled histogram is the non-NC $1\pi^0$ background and the hatched histogram is the additional contribution from wrong-sign neutrino induced NC $1\pi^0$ production. (b) The reconstructed π^0 angle distribution in neutrino running. (c) The reconstructed π^0 momentum distribution in antineutrino running. (d) The reconstructed π^0 angle distribution in antineutrino running.

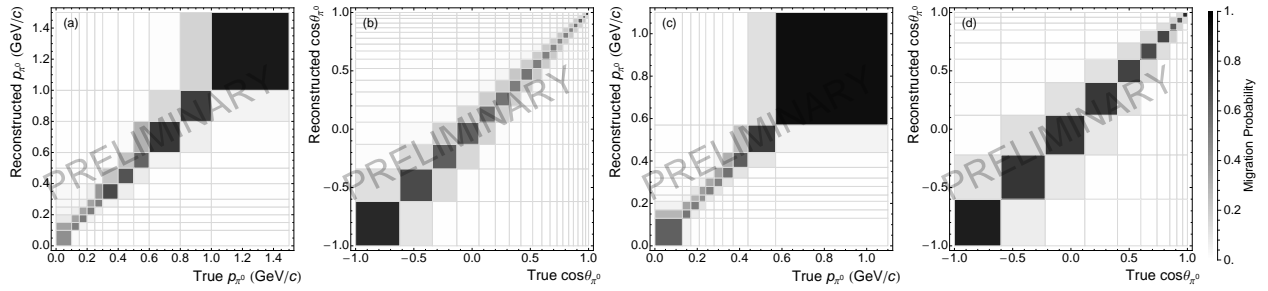


FIGURE 3. (a) Response matrix for the measurement of π^0 momentum in NC $1\pi^0$ events satisfying selection cuts in neutrino running. (b) The same for π^0 angle in neutrino running. (c) The same for π^0 momentum in antineutrino running. (d) The same for π^0 angle in antineutrino running.

mode. At 57% of the background, NC $1\pi^0$ events induced by wrong-sign¹ (WS) neutrinos are the dominant background in antineutrino mode. The same source comprises only 5% of the background in neutrino mode. Virtually all right-sign (RS) neutrino backgrounds consist of events in which at least one π^0 was produced in the detector. The π^0 can be produced in the struck nucleus or elsewhere in the tank via a charged pion undergoing charge exchange. Additionally, the exclusive NC $1\pi^0$ production channels can be classified as background if FSI induce the production of multiple π^0 s in the struck nucleus. In all, Monte Carlo predicts the contribution of each channel to the background in neutrino(antineutrino) mode to be: 23%(13%) from NC π^\pm production, 15%(5%) from CC π^\pm production, 10%(3%) from CC π^0 production, 13%(5%) from multi-pion production, 12%(7%) from NC elastic scattering, 5%(2%) from NC resonant $1\pi^0$ production, 3%(1%) from DIS, 5%(1%) from CC quasi-elastic scattering, 5%(2%) from K, ρ, η production, and the remainder from $\nu_e(\bar{\nu}_e)$ -induced signal and other interactions. The predicted absolutely normalized (normalized to POT) background is subtracted from each bin in each kinematic distribution. To subtract the WS background, the content of each bin is scaled by the predicted RS fraction in that bin.

Detector effects and biases in the reconstruction cause the measured π^0 kinematics to randomly deviate from their values. The *response matrix*, \mathbf{R} , encapsulates these effects. For a measurement, x , and a partition of the domain of x , (X_n) , R_{ij} is the probability that the reconstructed value of x is in bin i of (X_n) if the true value of x is in bin j (of not necessarily the same partition). The Monte Carlo estimated response matrices for the measurement of π^0 momentum and π^0 angle in neutrino and antineutrino mode appear in Figure 3. We find that the measured π^0 momentum tends to be overestimated, particularly at lower momentum. Fortunately, the measurement of π^0 angle appears to suffer from little to no bias and demonstrates very good resolution in the forward direction. We correct for the measurement distortion in a process known as unsmearing (or unfolding). Since each measurement differs from the others in some way, *e.g.* size of statistics, the distribution shape, and the form of the response matrix, applying the same unsmearing technique to

¹ Wrong-sign neutrinos are $\bar{\nu}_\mu$ in neutrino mode and ν_μ in antineutrino mode

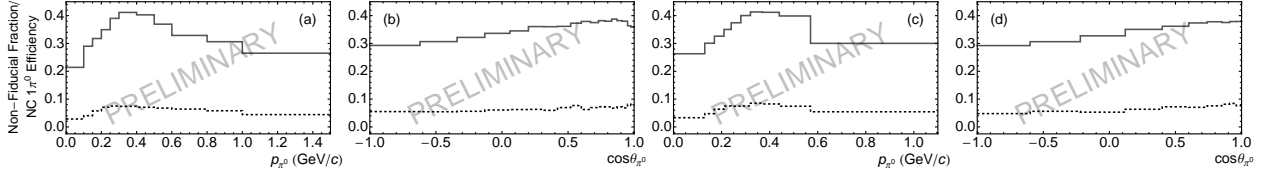


FIGURE 4. (a) NC $1\pi^0$ selection efficiency (solid line) and fraction of events reconstructed in the fiducial volume with true vertices outside the fiducial volume (dashed line) as a functions of π^0 momentum in neutrino running. (b) The same for π^0 angle in neutrino running. (c) The same for π^0 momentum in antineutrino running. (d) The same for π^0 angle in antineutrino running.

each distribution may not yield the best results. We have chosen to evaluate multiple options for unsmearing. Among the options are: (1) applying Tikhonov regularized unsmearing with the regularization strength chosen by the SVD prescription detailed by Höcker and Kartvelishvili[8], (2) applying a method analogous to one iteration of a Bayesian approach described by D’Agostini[9], and (3) applying no unsmearing. We have purposely omitted the matrix inversion technique because of its instability. Method (2) is modified to preserve the normalization of the distributions. For each measurement, we apply each unsmearing technique and choose the least-biased result. Method (1) is applied to the $\nu_\mu p_{\pi^0}$ distribution, method (2) to the $\nu_\mu \cos \theta_{\pi^0}$ and $\bar{\nu}_\mu p_{\pi^0}$ distributions, and method (3) to the $\bar{\nu}_\mu \cos \theta_{\pi^0}$ distribution.

The next set of corrections compensate for detector inefficiencies and misreconstruction. First, we correct for those events that actually occur outside the fiducial volume but are reconstructed inside of it. The number of events in the fiducial volume is overestimated by 7% because of a tendency of the reconstruction to pull interaction vertices to the center of the detector. The distributions are scaled by the fraction of true fiducial events in each bin. Second, we correct for the loss of signal events that do not satisfy the selection cuts. The average NC $1\pi^0$ selection efficiency is 36% in both neutrino and antineutrino mode. Both of these corrections appear in Figure 4. Notice that the selection efficiency is momentum dependent. The diminished efficiency at low momentum owes to the diminished ability of the $\log(\mathcal{L}_e/\mathcal{L}_\mu)$ cut to discriminate events. The diminished efficiency at high momentum owes to greater proportion of events failing the veto PMT hits cut (events are uncontained). The distributions are scaled by the inverse of the efficiency in each bin to recover the total rate of signal events.

The flux at MiniBooNE is predicted using a GEANT4-based simulation of the neutrino beam[2]. The simulation predicts a flux of $(33.5 \pm 4.3_{\text{sys}}) \times 10^{11} \nu_\mu/\text{cm}^2$ over the course of neutrino running and $(9.0 \pm 1.2_{\text{sys}}) \times 10^{11} \bar{\nu}_\mu/\text{cm}^2$ over antineutrino running. Each differential rate is divided by the appropriate integrated flux to determine the cross section.

The systematic uncertainty in the measured cross sections is taken to be the covariance of the cross sections measured under a programmatic set of Monte Carlo excursions wherein parameters underlying the simulation are varied within their uncertainties and correlations. The uncertainties can be grouped into three principal categories—cross section, flux, and detector. Cross section uncertainties relate to the assumed cross sections used in the Monte Carlo (predominately affects the background prediction). These uncertainties include errors on neutrino interactions as well as pion interactions both inside and outside the target nucleus. Flux uncertainties include uncertainties on meson production cross sections in the target, hadronic interactions in the target, the field produced by the magnetic horn, and POT counting. Uncertainties on the model of the production and propagation of light in the detector, PMT response, and bias in the unsmearing make up the detector uncertainty. In neutrino(antineutrino) mode, we asses an 8.1%(7.2%) cross section uncertainty, a 12.4%(13.5%) flux uncertainty, and a 5.6%(5.1%) detector uncertainty on the total NC $1\pi^0$ cross sections.

The measured absolute differential cross sections for NC $1\pi^0$ production after acceptance and efficiency corrections appear in Figure 5. These cross sections are flux-averaged; hence, they are specific to the neutrino flux at MiniBooNE. Per our signal definition, these cross sections include the effects of final state interactions. Integrating the differential cross sections yields total cross sections of $(4.73 \pm 0.05_{\text{stat}} \pm 0.40_{\text{sys}}) \times 10^{-40} \text{cm}^2/\text{nucleon}$ for ν_μ -induced production and $(1.42 \pm 0.05_{\text{stat}} \pm 0.14_{\text{sys}}) \times 10^{-40} \text{cm}^2/\text{nucleon}$ for $\bar{\nu}_\mu$ -induced production. Being the first absolute measurements of NC $1\pi^0$ production, we have no other measurements with which to compare these.

RESONANT CROSS SECTION & MODELS OF COHERENT PRODUCTION

Our measurement of NC $1\pi^0$ production was designed to be as model dependent as possible by choosing a signal definition that encompasses all possible sources of single π^0 production, including production through FSI and

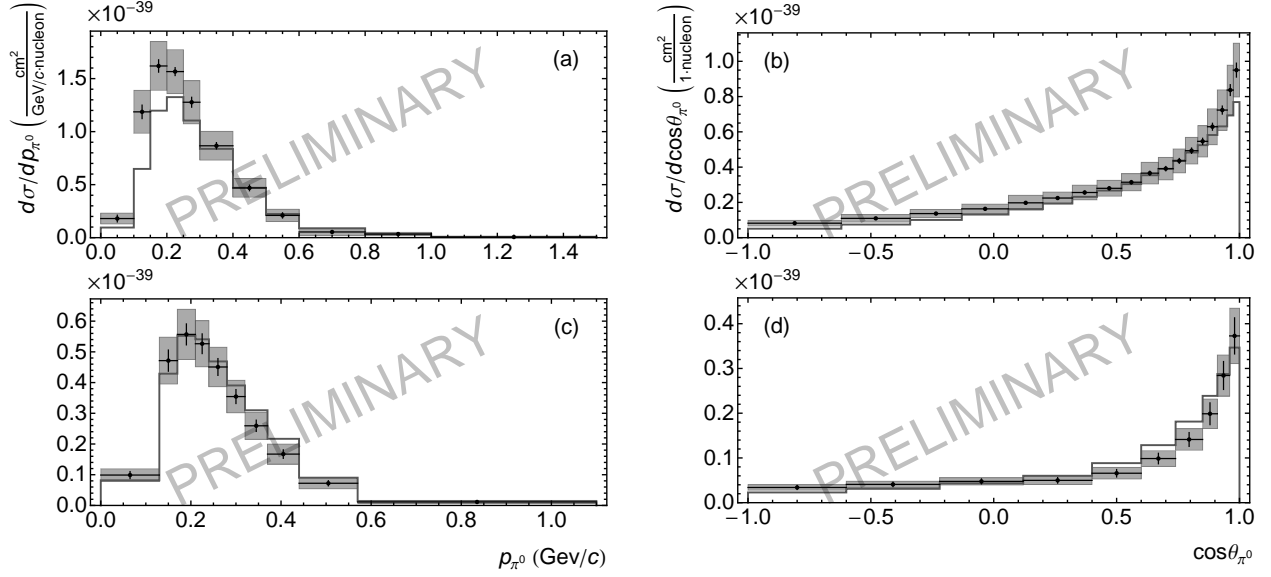


FIGURE 5. Flux-averaged absolute differential cross sections for NC $1\pi^0$ production on CH_2 . Data are shown as black dots with statistical error bars and systematic error boxes. The dark-gray line is the Monte Carlo prediction. (a) $\frac{d\sigma}{dp_{\pi^0}}$ for ν_μ -induced production. (b) $\frac{d\sigma}{d\cos\theta_{\pi^0}}$ for ν_μ -induced production. (c) $\frac{d\sigma}{dp_{\pi^0}}$ for $\bar{\nu}_\mu$ -induced production. (d) $\frac{d\sigma}{d\cos\theta_{\pi^0}}$ for $\bar{\nu}_\mu$ -induced production.

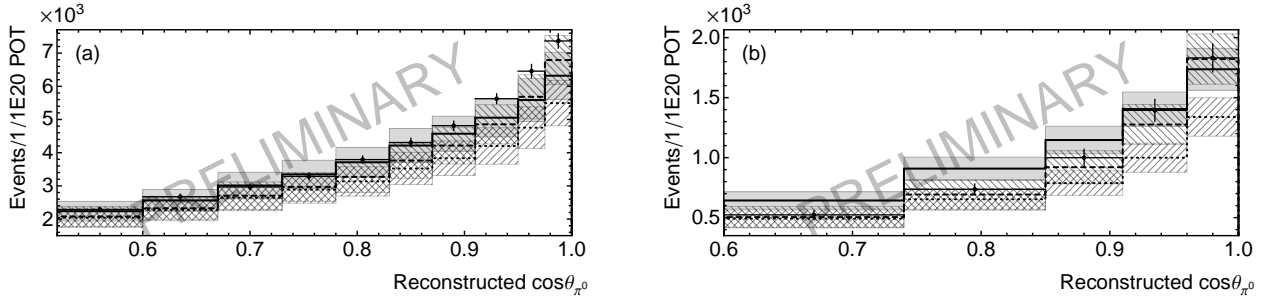


FIGURE 6. (a) The angular distribution in the forward region for NC $1\pi^0$ candidates in neutrino mode. Data is indicated by black dots with statistical error bars. Distributions are absolutely normalized to 10^{20} POT. The Monte Carlo prediction using the R-S model of NC coherent π^0 production is indicated by the solid black line with gray systematic error boxes. The prediction using the model of [10] is indicated by the dotted line with forward-hatched systematic error boxes. The dashed line with backward-hatched systematic error boxes is the prediction using the model of [11]. (b) The same for antineutrino mode.

coherent pion production mechanisms. Models of NC coherent π^0 production demonstrate wide variability in their predictions[10, 11]. Using the predictions for coherent production at MiniBooNE from the authors of [10] and [11], we have generated predictions of the angular distribution of events passing selection cuts under each model. The angular distribution is more sensitive to changes in coherent production, especially the antineutrino mode distribution because of the enhanced coherent production in that mode. Both [10] and [11] predict a sharper peak in the forward direction than the R-S model. This trend is evident in data as well. The markedly lower prediction of [10] illustrates the wide differences among the models.

A measurement of the NC resonant $1\pi^0$ cross section is particularly susceptible to variations in the assumed model of coherent pion production. Calculating this cross section requires the subtraction of coherent interactions. We also correct for FSI[3] so that the resulting cross section measures production at the struck nucleon rather than at the struck nucleus. We measure the resonant cross section assuming the MiniBooNE treatment of the R-S coherent model, the model from [10], and the model from [11], which yielded total cross sections of $(5.67 \pm 0.08_{stat} \pm 0.76_{sys}) \times 10^{-40} \text{ cm}^2/\text{nucleon}$, $(6.48 \pm 0.08_{stat} \pm 0.81_{sys}) \times 10^{-40} \text{ cm}^2/\text{nucleon}$, and $(6.08 \pm 0.08_{stat} \pm 0.78_{sys}) \times$

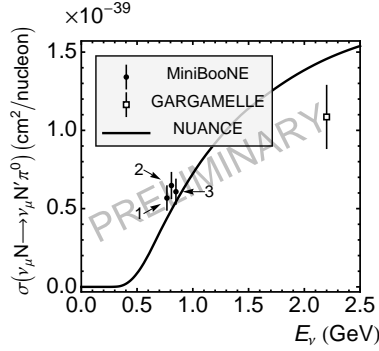


FIGURE 7. The flux-averaged total cross sections for ν_μ -induced resonant NC π^0 production corrected for FSI after subtracting out the predicted coherent contribution. Points 1, 2, and 3, are the cross sections extracted using the MiniBooNE implementation of the R-S model for coherent production, the model from [10], and the model from [11]. The points are placed at the mean energy of the beam in neutrino mode; the spread is only for clarity. The curve is the NUANCE prediction using the R-S resonant model. Also shown for comparison is the measurement made from GARGAMELLE data[12].

$10^{-40} \text{ cm}^2/\text{nucleon}$, respectively. These results appear in Figure 7 together with the NUANCE R-S prediction of resonant production and the only prior absolute measurement of resonant production on both protons and neutrons.

CONCLUSION

MiniBooNE has recorded the largest sample of neutrino and antineutrino-induced NC π^0 production interactions to date. Using this sample of events, we have measured flux-averaged absolute differential NC π^0 production cross sections as functions of both π^0 angle and π^0 momentum. In particular, we find the total cross section for ν_μ -induced production to be $(4.73 \pm 0.05_{\text{stat}} \pm 0.40_{\text{sys}}) \times 10^{-40} \text{ cm}^2$ at a mean energy of 808 MeV and for $\bar{\nu}_\mu$ -induced production to be $(1.42 \pm 0.05_{\text{stat}} \pm 0.14_{\text{sys}}) \times 10^{-40} \text{ cm}^2$ at a mean energy of 630 MeV. These results will be invaluable in constraining π^0 -related background for future ν_e -appearance oscillation searches using Cherenkov detectors and in testing models of coherent pion production.

REFERENCES

1. A. A. Aguilar-Arevalo, et al., *Nucl. Instrum. Meth.* **A599**, 28–46 (2009), 0806.4201.
2. A. A. Aguilar-Arevalo, et al., *Phys. Rev.* **D79**, 072002 (2009), 0806.1449.
3. D. Casper, *Nucl. Phys. Proc. Suppl.* **112**, 161–170 (2002), hep-ph/0208030.
4. D. Rein, and L. M. Sehgal, *Ann. Phys.* **133**, 79 (1981).
5. D. Rein, and L. M. Sehgal, *Nucl. Phys.* **B223**, 29 (1983).
6. A. A. Aguilar-Arevalo, et al., *Phys. Lett.* **B664**, 41–46 (2008), 0803.3423.
7. R. Patterson, E. Laird, Y. Liu, P. Meyers, I. Stancu, and H. Tanaka, *Nuclear Instruments and Methods in Physics Research Section A: Accelerators, Spectrometers, Detectors and Associated Equipment* **608**, 206–224 (2009), ISSN 0168-9002.
8. A. Höcker, and V. Kartvelishvili, *Nucl. Instrum. Meth.* **A372**, 469–481 (1996), hep-ph/9509307.
9. G. D’Agostini, *Nuclear Instruments and Methods in Physics Research Section A: Accelerators, Spectrometers, Detectors and Associated Equipment* **362**, 487–498 (1995), ISSN 0168-9002.
10. J. E. Amaro, E. Hernández, J. Nieves, and M. Valverde, *Physical Review D (Particles and Fields)* **79**, 013002 (2009).
11. L. Alvarez-Ruso, L. S. Geng, and M. J. V. Vacas, *Physical Review C (Nuclear Physics)* **76**, 068501 (2007).
12. E. A. Hawker, “Single Pion Production in Low Energy ν -Carbon Interactions,” in *Proceedings of the 2nd International Workshop on Neutrino Nucleus Interactions in the Few GeV Region*, edited by G. P. Zeller, 2002, available at <http://www.ps.uci.edu/~nuint/proceedings/hawker.pdf>.